

# Density functional theory study of $\text{CH}_x$ ( $x=1-3$ ) adsorption on clean and CO precovered Rh(111) surfaces

Ming-Mei Yang

State Key Laboratory Of Catalysis, Dalian Institute of Chemical Physics, Chinese Academy of Sciences, 457 Zhongshan Road, Dalian 116023, China and Graduate School of the Chinese Academy of Sciences, Beijing 100039, China

Xin-He Bao

State Key Laboratory Of Catalysis, Dalian Institute of Chemical Physics, Chinese Academy of Sciences, 457 Zhongshan Road, Dalian 116023, China

Wei-Xue Li<sup>a)</sup>

State Key Laboratory Of Catalysis, Dalian Institute of Chemical Physics, Chinese Academy of Sciences, 457 Zhongshan Road, Dalian 116023, China and Center for Theoretical and Computational Chemistry, Dalian Institute of Chemical Physics, Chinese Academy of Sciences, 457 Zhongshan Road, Dalian 116023, China

(Received 12 January 2007; accepted 28 May 2007; published online 12 July 2007)

$\text{CH}_x$  ( $x=1-3$ ) adsorptions on clean and CO precovered Rh(111) surfaces were studied by density functional theory calculations. It is found that  $\text{CH}_x$  ( $x=1-3$ ) radicals prefer threefold hollow sites on Rh(111) surfaces, and the bond strength between  $\text{CH}_x$  and Rh(111) follows the order of  $\text{CH}_3 < \text{CH}_2 < \text{CH}$ . A slight attraction between adsorbed  $\text{CH}_x$  and  $\text{CH}_x$ ,  $\text{CH}_x$  and CO, CO and CO radicals/molecules at coverage of  $1/9-1/4$  ML is found, and considerable repulsion is built up at coverage higher than  $1/4$  ML. It is found that  $\text{CH}_x$  adsorption results in the reduction of work function due to charge transfer from the adsorbates to the substrate. For  $\text{CH}_3$  adsorption, charge accumulation between the substrate and carbon atom is identified, which results in C–H stretch mode softening. For CO precovered surfaces, the mode softening is prevented due to the weakened interaction between  $\text{CH}_x$  and substrates from repulsive interaction between adsorbates. Conversely, the overall charge transfer from the  $\text{CH}_x$  ( $x=1-3$ ) to the substrate enhances the charge back donation from the substrate to the empty antibonding states of adsorbed carbon monoxide, which results in the softness of the C–O stretch, respectively. The C 1s surface core-level shifts for  $\text{CH}_x$  with and without the presence of CO were calculated, and a negative shift with respect to the carbon in atop CO on Rh(111) is found, and the negative shift follows the order of  $\text{CO} < \text{CH}_3 < \text{CH}_2 < \text{CH}$ . The results are analyzed in details by difference of charge density and projected density of states. © 2007 American Institute of Physics. [DOI: 10.1063/1.2751155]

## I. INTRODUCTION

Methane dissociation and activation on catalyst is one of the most important industry process due to its great relevance for utilization of natural gas, which attracts great interest in decades. Among of them, rhodium is a unique catalyst due to its high selectivity and activity for methane partial oxidation or steam reforming to synthesis gas (a mixture of carbon monoxide and hydrogen), and subsequently the synthesis of higher oxygenated hydrocarbons for clean fuels and chemical feedstocks, in particular. For the synthesis of higher oxygenated hydrocarbon, the reaction begins with CO dissociation and hydrogenation to produce  $\text{CH}_x$  species, which then undergo either hydrogenation to produce  $\text{CH}_4$  or chain growth with another  $\text{CH}_x$  to produce  $\text{C}_2$  hydrocarbon, or CO insertion to produce  $\text{C}_2$  oxygenates.<sup>1-3</sup> The activity and selectivity of  $\text{C}_2$  oxygenates on Rh-based catalysts have been attributed to their ability for catalyzing CO dissociation and

CO insertion. Concerning CO dissociation on Rh, previous studies have shown that it is negligible on close packed Rh(111), Rh(110), and Rh(100) surfaces.<sup>4</sup> However, the efficiency can be improved significantly at kinked step edges where Rh atoms have the lowest coordination.<sup>5</sup> To uncover the mechanism for CO insertion of  $\text{CH}_x$  ( $x=1-3$ ) to produce  $\text{C}_2$  oxygenates, the interaction between CO and  $\text{CH}_x$  ( $x=1-3$ ) and characterization in terms of the adsorption sites, energetics, as well spectroscopy (electronic and vibrational) are essential, and will be addressed in present work. Since Rh(111) has the lowest surface energy and therefore being the most abundant surfaces, it was selected as prototype system.

Experimental characterization for  $\text{CH}_x$  species adsorption on transition metal surfaces has been focused mainly on methyl ( $\text{CH}_3$ ) so far.<sup>6-11</sup> The adsorption and reaction of methyl groups have been generated by the pyrolysis of azomethane ( $\text{CH}_3\text{N}_2\text{CH}_3$ ) on clean and CO-modified Rh(111).<sup>10</sup> It was found that the temperature for the disappearance of asymmetric vibration of  $\text{CH}_3$  species increased

<sup>a)</sup> Author to whom correspondence should be addressed. Electronic mail: wxli@dicp.ac.cn

from 300 to 475 K after preadsorbed CO. This demonstrated that the stability of adsorbed methyl groups has been enhanced by CO, and the reason for the stabilization has been attributed to the site blocking and electronic effect.<sup>10</sup> Due to the high reactivity of CH<sub>2</sub> and CH radicals, they were generated normally via corresponding iodo compounds and have been studied by temperature-programmed desorption (TPD), x-ray photoelectron spectroscopy (XPS), reflection absorption infrared spectroscopy (RAIRS), and high-resolution electron energy loss spectroscopy.<sup>11–13</sup> Formation of CH<sub>x</sub> ( $x=1-3$ ) has been suggested by decomposition of ethanol on Rh(111) using real-time XPS and TPD,<sup>14</sup> where various C 1s peaks observed were attributed to various intermediates, but detail assignments remained. In the present work, the surface core-level shifts of carbon in CH<sub>x</sub> and CO are calculated and compared with available experimental data.

Adsorption induced vibrational mode softening/redshift stimulated wide interests due to its potential relationship to the surface reactivity.<sup>15–24</sup> The mechanism behind is thought to be charge transferring from the substrate to the adsorbed molecules, which can be modified further by the coadsorption of other species with different electron negativities to prevent or facilitate the charge transferring. For methyl adsorption on Rh(111) surface, the C–H stretch ( $\nu(\text{CH})$ ) mode softening has been found only when it adsorb on the hollow site.<sup>24</sup> When methyl is coadsorbed with oxygen, however, the softening was prevented, as shown both experimentally<sup>6</sup> and theoretically.<sup>25</sup> Similar to this, for CO adsorption on Rh(111), the redshift for C–O stretch mode was seen to shift toward higher wave numbers with the presence of oxygen in RAIRS experiments and density functional theory (DFT) calculations.<sup>26</sup> Interestingly, when CO and methyl adsorb simultaneously on the Rh(111) surface, the redshift of CO stretching was found.<sup>10</sup> The detail mechanism behind will be discussed in the present paper.

Theoretically, CH<sub>x</sub> radical adsorption on transition metal (TM) surfaces has been extensively studied in the past.<sup>14,22,25,27–41</sup> CH<sub>x</sub> adsorptions on Pt(111), Pd(111), and Rh(111) surfaces were studied using a cluster model.<sup>31–33</sup> In these papers, it was found that the adsorbed hydrocarbons tend to maintain the tetrahedral coordination, i.e., CH, CH<sub>2</sub>, and CH<sub>3</sub> prefer threefold hollow site, twofold bridge site, and onefold top site, respectively. Similar results have been found on the Pt(111) surface by periodic plane wave slab model.<sup>15,28</sup> The preference of the tetrahedral coordination in these metals may come from their nobleness, whose *d* bands are nearly full. When it comes to TM surfaces in the left of the Periodic Table, the *d*-band occupancy decreases and the hybridization between *d* band and adsorbed molecules increases, the high coordination configurations are preferred, correspondingly. Indeed, for Rh(111),<sup>24,25</sup> Ru(0001),<sup>29,30</sup> Cu(111),<sup>15,38,39</sup> and Ni(111),<sup>40</sup> CH<sub>3</sub> has been found to adsorb on high-coordinated threefold hollow site. In present paper, CH<sub>2</sub> and CH adsorptions on Rh(111) surface with and without the presence of the CO are studied using periodic plane wave slab model, and one of our goal is therefore to make clear whether the preference of the high coordination site is maintained.

The paper is organized as follows. Computational details

are described in Sec. II. In Sec. III, the energetics and geometries for CH<sub>x</sub> ( $x=1-3$ ) with/without the presence of preadsorbed CO are studied. It is followed in Sec. IV by a brief discussion on the effect of coverage and the energy diagram related to methane dissociation. The calculated C 1s surface core level shift (SCLS) and work functions are presented in Sec. V, and detailed analyses of the vibration spectroscopy and affect of precovered CO are performed in Sec. VI. Electronic structures are studied in terms of the projected density of states and the difference of electron density in Sec. VII, and summary is given in Sec. VIII at last.

## II. METHODS

All calculations are carried out using self-consistent DFT, which has been implemented in “DACAPO,” a highly optimized ultrasoft pseudopotential plane wave package.<sup>42,43</sup> The Kohn-Sham one-electron valence states are expanded by plane waves with kinetic energies up to 25 Ry, and a Monkhorst-Pack mesh ( $4 \times 4 \times 1$ ) grids for ( $2 \times 2$ ) supercell and ( $2 \times 2 \times 1$ ) for ( $3 \times 3$ ) supercell are used for surface Brillouin zone sampling. The exchange-correlation approximation are described by generalized gradient approximations self-consistently for GGA-PW91,<sup>44</sup> and non-self-consistently for revised Perdew-Burke-Ernzerhof (RPBE).<sup>42</sup> The self-consistent density is determined by iterative diagonalization of the Kohn-Sham Hamiltonian with Fermi population of the Kohn-Sham states ( $k_B T=0.1$  eV) and Pulay mixing of the resulting electronic density.

The calculated lattice constant, 3.83 Å, which agrees well with the experimental bulk lattice constant of 3.80 Å, has been employed throughout the paper. Gas-phase calculations are carried out in a  $10.0 \times 10.2 \times 10.3$  Å<sup>3</sup> unit cell and the Brillouin zone is sampled with one *k* point. The Rh(111) surfaces are modeled by a five-metal-layer slab, periodically repeated in a supercell geometry separated by 13 Å of vacuum. The chemisorbed species and metal atoms in the top layer are fully optimized until the residual forces are smaller than 0.02 eV/Å. The atoms in the bottom four layers are fixed at their corresponding bulk truncated positions. Spin polarization has been included during the iteration for both the gas-phase radical species and the adsorbate-substrate system. Adsorption is allowed on one side of the metal slabs, and the electrostatic potential is adjusted by applying a dipole correction in the vacuum.<sup>45</sup>

The vibrational spectra calculations are based on the numerical calculation of the second derivatives of the potential energy surface within the harmonic approach.<sup>46</sup> To exclude possible effect of the residual forces on the calculation of the vibration frequency (hereby the force constant), the structures have been optimized thoroughly until the residual forces are less than 0.005 eV/Å. The displacement for geometrical perturbation, 0.02 Å, is chosen in present paper, to keep the harmonic approximation. [Decreasing the displacement to the 0.01 Å, the variation of the calculated frequency for CO adsorption on top site of Rh(111) at 1/4 ML, for example, is less than  $\sim 3$  cm<sup>-1</sup>.] The calculated stretching frequency for gas-phase CO molecule, 2201 cm<sup>-1</sup>, agrees well with the results from GAUSSIAN, 2210 and

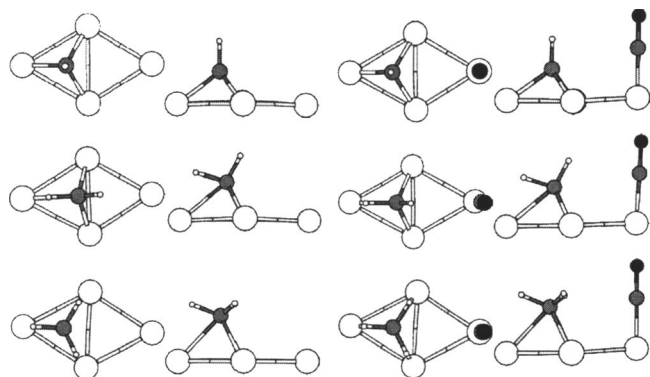


FIG. 1. Schematic plot (top and site view) for the adsorbed CH<sub>x</sub> species without (left column) and with (right column) the presence of CO. The gray and black circles represent carbon and oxygen atoms, and the large (small) white circles represent Rh (H) atoms, respectively. For simplicity, only Rh(111) atoms in topmost layer are shown.

2211 cm<sup>-1</sup>,<sup>47–49</sup> and the experimental (harmonic) data at 2170 cm<sup>-1</sup>.<sup>50</sup>

By definition, the binding energy of the specific core-level electron,  $E_{BE}$ , can be calculated by

$$E_{BE} = E(n_c - 1) - E(n_c), \quad (1)$$

where  $E(n_c)$  and  $E(n_c - 1)$  are the total energies from DFT before and after core electron is excited from specific atoms. To calculate  $E(n_c - 1)$ , a pseudopotential with core hole has been generated, and the removed electron has been placed to the Fermi level of the system to maintain the neutrality of system. Since the  $E_{BE}$  is element specific and sensitive to the environment, it is used as fingerprint to probe oxidic states and adsorption sites. The difference of  $E_{BE}$ , the so-called surface core-level shift (SCLS), can be compared to corresponded experimental data to identify the adsorption sites and local geometry.<sup>51–53</sup>

### III. GEOMETRIES AND ENERGETICS

To examine the preferences of CH<sub>x</sub> (x=1–3) fragments on Rh(111) surfaces, various sites—top, bridge, fcc-hollow and hcp-hollow sites—were studied in detail. For CH<sub>3</sub> and CH<sub>2</sub> species, there are two possible configurations with different azimuthal orientations: C–H bonds pointing toward the nearest-neighbor Rh atoms (noted as top-H) and midway between two neighboring Rh atoms in the top layer (noted as bri-H). Accordingly, the adsorption geometry, for example,

fcc/top-H means CH<sub>x</sub> adsorbs at fcc-hollow site with C–H bond point toward the nearest-neighbor Rh atoms. The optimized structures for adsorbed CH<sub>x</sub> with and without the presence of CO have been shown schematically in Fig. 1.

#### A. CO adsorption

It is well known that present DFT predicts wrong CO adsorption sites on Pt(111) and Rh(111) surfaces at low coverages.<sup>27,52–57</sup> Our calculated binding energies for CO adsorption on Rh(111) surfaces are listed in Table I, where the results for both of PW91 and RPBE functionals are given. As seen in Table I, the energy difference between various sites is less than 0.11 eV by PW91 and 0.13 eV by RPBE, which indicates the small corrugation of the potential energy surface. By PW91 functional the hcp-hollow site is energetically favorable; while atop site adsorption is preferred by RPBE. Thus, the RPBE functional gives a better description for CO adsorption on Rh(111), which is consistent with previous results for CO adsorption on Rh and Pt(111).<sup>55,58</sup> For atop site adsorption, CO stands perpendicularly to the surface with Rh–C bond length being 1.82 Å and C–O bond length being 1.17 Å, which agree well with previous generalized gradient approximation (GGA) studies.<sup>52,53</sup>

#### B. CH<sub>x</sub> (x=1–3) adsorption

The calculated energetical results for CH<sub>x</sub> adsorption at 1/4 ML coverage are given in Table I, where various configurations optimized by different functionals have been considered. For CH<sub>3</sub> adsorption, it has been found that C–H bond prefers to point toward nearest-neighbor Rh atoms (top-H) rather than middle way between nearest-neighbor Rh atoms (bri-H), irrespective the adsorption site (top or hollow site) and exchange-correlation functional used. It indicates that a barrier may exist to hinder the methyl in-plane rotation. Among all of the possible adsorption sites (fcc, hcp, atop, and bridge), fcc-hollow sites are the energetically most favorable from PW91. Nevertheless, the energy difference between various sites is less than 0.05 eV for top-H direction, which reflect the flatness of the potential energy surface of CH<sub>3</sub> on Rh(111) surfaces. Using five-layer slab and PW91/PBE functional, Xiao and Xie<sup>24</sup> and Walter and Rappe<sup>25</sup> found fcc-hollow site preference, which agree with the present calculations. When RPBE is applied, the present calculations show that atop site is energetically most favor-

TABLE I. Binding energies (in eV) for CO and CH<sub>x</sub> radicals on Rh(111) surfaces calculated by PW91 (RPBE in parenthesis) within (2×2) cell. NS means a site which is not stable. The most stable sites are indicated by bold font.

	Atop		Bridge	fcc		hcp	
	Top-H	Bri-H		Top-H	Bri-H	Top-H	Bri-H
CO	-2.08 (-1.76)		-2.03(-1.65)	-2.02 (-1.63)		<b>-2.13</b> (-1.74)	
CH	-4.63 (-4.22)		NS	-6.49 (-6.03)		<b>-6.67</b> (-6.20)	
CH <sub>2</sub>	-3.23 (-2.86)	-3.22 (-2.85)	-3.95 (-3.52)	-3.95 (-3.47)	<b>-4.07</b> (-3.58)	-3.96 (-3.48)	NS
CH <sub>3</sub>	-1.76 ( <b>-1.42</b> )	-1.75 ( <b>-1.42</b> )	-1.71 (-1.28)	<b>-1.78</b> (1.29)	-1.37 (-0.95)	-1.73 (-1.25)	NS
	<b>-1.82<sup>a</sup></b>	<b>-1.82<sup>a</sup></b>	NS	-1.83 <sup>a</sup>	-1.47 <sup>a</sup>	-1.76 <sup>a</sup>	-1.40 <sup>a</sup>

<sup>a</sup>Reference 24.

TABLE II. Main structural parameters (distance in Å and angle in deg) for  $\text{CH}_x$  radicals on clean and CO precovered Rh(111) surface within  $(2 \times 2)$  cell. The arabic number in subscript indicates the number of bond with same bond length.

	Favorable site	$d_{\text{Rh-C}}$	$d_{\text{C-H}}$	$d_{\text{Rh-H}}$	$h_{\text{C-surf}}$
Rh(111)					
CH	hcp	1.98	1.10	...	1.16
	fcc	1.98	1.10	...	1.12
$\text{CH}_2$	fcc/bri-H	$2.02_{\times 2}, 2.20$	1.10, 1.19	$1.84, 2.68_{\times 2}$	1.35
$\text{CH}_3$	top/top-H	2.09	1.10	2.65	2.26
	fcc/top-H	$2.27_{\times 2}, 2.26$	1.10	2.13	1.63
Co precovered					
Rh(111)					
CH	fcc	$1.97_{\times 2}, 1.98$	1.10	...	1.21
	hcp	1.98	1.10	...	1.16
$\text{CH}_2$	fcc/bri-H	$2.02_{\times 2}, 2.22$	1.10, 1.18	$1.86, 2.70_{\times 2}$	1.37
$\text{CH}_3$	fcc/top-H	2.28	1.12	2.16	1.65

able and 0.17 eV lower than the least stable hcp-hollow site. These results are well converged with respect to the  $k$ -point sampling and plane wave cutoff: the variation of relative energetics is around few meV by increasing the  $k$ -point sampling from Monkhorst-Pack grid  $(4 \times 4 \times 1)$  to  $(6 \times 6 \times 1)$  and  $(8 \times 8 \times 1)$  and plane wave cutoff from 340 to 380 and 400 eV, respectively. However, the relative stability is sensitive to the thickness of slab: if a thinner slab was used, for example, three-layer slab to five-layer slab, which may include artificially size effect, the reversal of the site preference is predicted by both functionals, as found by the present and previous calculations.<sup>27</sup> As seen from following vibrational analysis, asymmetric stretching mode  $\nu_{\text{as}}(\text{CH}_3)$  softness observed by experiments<sup>10</sup> can be obtained only if methyl adsorb at fcc-hollow site, which is predicted by PW91 (instead of RPBE) functional when the calculations are well converged. Correspondingly, PW91 is adopted self-consistently throughout the present paper. For reference, non-self-consistent PRBE results are given.

Structural parameters for the favorable  $\text{CH}_3$  fcc site adsorption are listed in Table II. Comparing to atop site adsorption, the C–Rh bond length increases from 2.09 to 2.26 Å, respectively. The C–H bond length in both structures is, however, less affected by adsorption with respect to the molecules in gas phase.

For  $\text{CH}_2$  adsorption, we found that both PW91 and RPBE predict the fcc-hollow site preference and is 120 and 60 meV more favorable than the bridge site, respectively. In the past, Koster and Van Santen calculated  $\text{CH}_2$  adsorption on Rh cluster at bridge site using extended Hückle method, where  $\text{CH}_2$  was assumed to be the bridge site.<sup>33</sup> For fcc-hollow site adsorption, as indicated in Fig. 1 and Table II, the carbon atom is 1.35 Å above the surface, where the carbon atom bonds to three Rh atoms with two types of inequivalent bonds: two are 2.02 Å and the remained one is 2.20 Å. Note that for the closest C–H bond to the surface, it is elongated to 1.19 Å, contrast to 1.10 Å in the gas phase, and the distance between corresponding H atom and the Rh atom underneath is 1.84 Å. Similar results have been obtained on Ni(111) surface by Watwe *et al.* using the periodic plane wave code

method, where methyl group was calculated to be located nearly symmetrically at the center of the hollow site.<sup>40</sup>

For CH adsorption, whose C–H bond points away from the surface, both the PW91 and RPBE calculations predict a hcp-hollow site preference. The geometry of CH adsorption has  $C3v$  symmetry, which agrees with previous DFT studies on Rh(111) and Ni(111).<sup>33,40</sup> The C atom sits 1.16 Å above the surface with the Rh–C bond length being 1.98 Å, and the C–H bond is intact with respect to the gas-phase radicals.

From the above results, it can be found that high coordination fcc-hollow sites are preferred for  $\text{CH}_x$  ( $x=1-3$ ) when PW91 is applied. Our calculations show that the magnitude of the binding energy of  $\text{CH}_x$  ( $x=1-3$ ) radicals is considerable, which is understandable due to the unsaturated lone-pair electron of the radicals. The smaller  $x$  in  $\text{CH}_x$  is (more reactive), the larger binding energy it has. Along with these, carbon atom in  $\text{CH}_x$  gets closer to the surfaces.

### C. $\text{CH}_x$ adsorption on CO precovered surface

For  $\text{CH}_x$  adsorption on CO precovered surface, only the configuration for CO adsorption at the atop site and  $\text{CH}_x$  ( $x=1-3$ ) adsorption at hollow site, as indicated by experiments, were considered and plotted schematically in Fig. 1. The calculated energetics are given in Table III, where the binding energies for  $\text{CH}_x$  radicals on the preadsorbed surfaces and the lateral interactions between two adsorbates,  $\Delta E$ , were calculated. For  $\Delta E$ , a positive value indicates a repulsive interaction between adsorbates and negative for attractive interaction. From Table III, it can be found that repulsive interactions are prevailed for all considered coadsorption systems at 1/4 ML coverage. For methyl and CO coadsorption, it is found that for methyl, fcc/top-H is energetically favorable. For  $\text{CH}_2$ , fcc/bri-H configuration is preferred. For these two radicals, both PW91 and RPBE functionals give same site preference. For CH adsorption, both functionals predict hollow site preference, though there is slight site difference (hcp site for PW91 and fcc for RPBE). The small energy difference (less than 0.1 eV) and functional dependence/uncertainty found here indicate that both sites may be populated with the presence of CO. Main structural parameters are given at bottom of Table II. Compared to

TABLE III. Binding energies (in eV) for CH<sub>x</sub> and lateral interactions ( $\Delta E$ ) on CO precovered Rh(111) surface calculated within PW91 (PRBE in parenthesis) with (2×2) cell. NS means a site which is not stable. The most stable sites are indicated by bold font.

		CH		CH <sub>2</sub>		CH <sub>3</sub>	
		BE	$\Delta E$	BE	$\Delta E$	BE	$\Delta E$
fcc	top-H	-6.30 ( <b>-5.89</b> )	0.19 (0.14)	-3.70 (-3.16)	0.25 (0.31)	<b>-1.54 (-0.99)</b>	0.24 (0.30)
	bri-H			<b>-3.82 (-3.29)</b>	0.25 (0.29)	NS	...
hcp	top-H	<b>-6.40</b> (-5.81)	0.27 (0.39)	-3.65 (-3.11)	0.31 (0.37)	-1.44 (-0.89)	0.29 (0.36)
	bri-H			-3.76 (-3.22)	0.30 (0.36)	-0.75 (-0.59)	0.98 (1.23)

clean Rh(111) without the presence of carbon monoxide, it can be seen that the height of carbon atom in CH<sub>x</sub> radicals is raised by 0.02–0.05 Å with the presence of CO, which are in line with the repulsive interactions between adsorbates.

## IV. DISCUSSION

### A. Effect of the coverage

The dependence on the coverage is studied in the present section using a large  $p(3 \times 3)$  supercell (1/9 ML). The calculated binding energies are given in Table IV, where the results at 1/4 ML coverage are listed in bracket for comparison. From Table IV, it can be found that the binding energy of CO decreases by 0.11 eV from 1/9 to 1/4 ML, which indicates an attractive interaction between adsorbed molecules at coverages of 1/9–1/4 ML. For CH<sub>x</sub> (x=1–3), a weak attraction between CH<sub>x</sub> (x=1–3), less than 0.03 eV, is found, too. When the coverage is higher than 1/4 ML, however, considerable repulsion is built up. Within (2×2) unit cell, for example, the (average) binding energy for methyl is -1.75 eV for 1/4 ML, -1.66 eV if additional methyl placed at atop site (1/2 ML), and -1.01 eV if all three methyl radicals placed at atop site (3/4 ML). The lateral interaction between coadsorbed CO and CH<sub>x</sub> molecules has been studied within the (3×3) unit cell as well, where one CH<sub>x</sub> (x=1–3) radical has been placed at the hollow site next to the atop-site CO. Compared to the coadsorption within the (2×2) unit cell, where a considerable repulsion has been found, a modest attraction (0.01–0.03 eV) is found.

Kecskés *et al.* studied the effect of preadsorbed CO on the surface chemistry of CH<sub>3</sub>/Rh(111) by RAIRS.<sup>10</sup> For CH<sub>3</sub>

adsorbed on Rh(111), the asymmetric stretching vibrations disappeared between 300 and 320 K. For the CO precovered surface, this temperature was approximately 475 K. The reason was attributed to either the possible stabilization by electronic effect or a site blocking effect by the presence of CO.<sup>10</sup> Our calculations at low coverage in the (3×3) unit cell may provide a mechanism for the stabilization, where the attractive interaction between CH<sub>3</sub> and CO (0.01–0.03 eV) corresponds to a temperature variation of 116–348 K. When coverage increases to 1/4 ML, significant repulsion is built up, as found by present calculations. In this case, site blocking effect may play the role and prevents the decomposition of CH<sub>3</sub>.

### B. CH<sub>4</sub> dissociation

Using the obtained energetics, the energy diagram for CH<sub>4</sub> dissociation with respect to gas-phase CH<sub>4</sub> with and without the presence of CO on Rh(111) surface within (2×2) unit cell can be deduced and plotted in Fig. 2. In the figure, dissociated products CH<sub>x</sub> have been placed on their most stable sites and excess H atoms on the separated slabs. From Fig. 2, it can be found that the first step of methane dissociation, namely, the formation of the CH<sub>3</sub> and H atom, is slightly endothermic on the clean substrate. Subsequent dissociation to CH<sub>2</sub>+2H and CH+3H, however, becomes exothermic. The reaction energies are 0.02 (0.57) eV (CH<sub>3</sub>+H), -0.21 (0.42) eV (CH<sub>2</sub>+2H), -0.83 (-0.16) eV (CH+3H), and -0.54 (0.23) eV (C+4H) for PW91 (RPBE), respectively. According to Brønsted-Evans-Polanyi-type relationship between the activation energy for dissociation and

TABLE IV. Binding energies, lateral interaction  $\Delta E$ , and core-level shift  $\Delta SCLS$  (in eV) for adsorbed CH<sub>x</sub> on clean and CO precovered Rh(111) surface within (3×3) cells. The value in the parentheses responds to the results calculated within (2×2) cell.

	Sites	BE(eV)	$\Delta E$	$\Delta SCLS$ (eV)
Rh(111)				
CO	top	-1.97 (-2.08)	...	
CH	hcp	-6.64 (-6.67)	...	-2.45 (-2.49)
CH <sub>2</sub>	fcc/bri-H	-4.03 (-4.07)	...	-2.16 (-2.21)
CH <sub>3</sub>	fcc/top-H	-1.75 (-1.78)	...	-1.75 (-1.67)
Co pre-covered Rh(111)				
CH	hcp	-6.67 (-6.40)	-0.03 (0.27)	-2.45 (-2.55)
CH <sub>2</sub>	fcc/bri-H	-4.04 (-3.82)	-0.01 (0.25)	-2.18 (-2.31)
CH <sub>3</sub>	fcc/top	-1.78 (-1.54)	-0.03 (0.24)	-1.82 (-1.85)

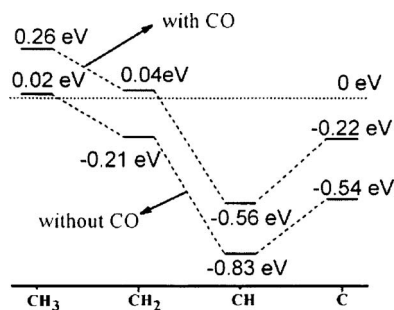


FIG. 2. Energy diagram for adsorbed  $\text{CH}_x$  with and without the presence of CO on Rh(111). The energy references are gas-phase  $\text{CH}_4$  and clean Rh(111) substrate. Excessed H atoms are placed at the energetically most favorable sites on a separate slab.

the binding energy of  $\text{CH}_x$  radicals,<sup>59–61</sup> the endothermic feature for the first C–H bond activation implies a significant barrier for the formation of  $\text{CH}_3$ , while the large energy drop for further decomposition indicates the dissociation to  $\text{CH}_2 + 2\text{H}$  and  $\text{CH} + 3\text{H}$  will be facile. The decomposition from  $\text{CH} + 3\text{H}$  to  $\text{C} + 4\text{H}$  is endothermic again, which means that a significant barrier may exist to prevent complete C–H decomposition. These results agree well with experimental and theoretical findings about the activation of methane on transition metal surfaces, where the scissors of the first C–H bond are the rate limiting step, and CH radical has been observed frequently as the stable species by various spectroscopes during the methane activation.<sup>30,40,62–64</sup> Our calculations show that with the presence of CO, the overall energetics are raised up due to the repulsion between the adsorbates, and reactivity is improved, respectively.

### V. C 1s SCLS AND WORK FUNCTION

Table V lists the calculated C 1s SCLS for adsorbed  $\text{CH}_x$  radicals, with respect to the carbon atom of atop CO on Rh(111) at 1/4 ML coverage. As a benchmark, the C 1s SCLSs for adsorbed CO at various sites were first calculated, and calculated SCLS between CO at atop and hollow site is 0.67 eV, which agrees well with previous calculations [0.68 eV (Ref. 52) or 0.72 eV (Ref. 53)] and experimental findings [0.69 eV (Ref. 65)].

For simplicity, only C 1s SCLSs of adsorbed  $\text{CH}_x$  at the energetically most favorable hollow sites with and without the presence of CO molecule are studied. On clean surfaces, all of the calculated C 1s SCLSs for  $\text{CH}_x$  ( $x=1-3$ ) are nega-

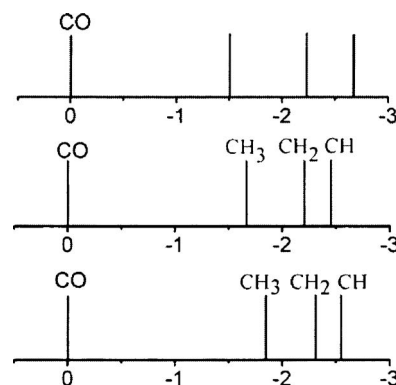


FIG. 3. Calculated C 1s core-level shift for  $\text{CH}_x$  radicals on clean (middle) and CO-modified (bottom) Rh(111) surface. The dash lines (top) are experimental data from Ref. 14. The energy reference corresponded to atop-site CO on clean Rh(111).

tive: the smaller  $x$ , the larger shift ( $-1.67$  eV for  $\text{CH}_3$ ,  $-2.21$  eV for  $\text{CH}_2$ , and  $-2.45$  eV for CH, respectively). With the presence of CO, the C 1s levels of  $\text{CH}_x$  have been further shift toward the lower energy, by 0.18 eV for  $\text{CH}_3$  and 0.10 eV for both  $\text{CH}_2$  and CH, respectively. Finally, we note that C 1s SCLSs are sensitive to the adsorption sites and can be varied in magnitude of 1 eV at different adsorption sites, which will be discussed elsewhere.

Using the real-time XPS technique, Vesselli *et al.* observed one C 1s peak appear at 284.4 eV for temperatures up to 400 K during the process of ethanol decomposition on Rh(111). Upon further increase of the temperature, the appearance of peaks at 283.7 and 283.2 eV peaks were observed.<sup>14</sup> These peaks were attributed to either  $\text{CH}_x$  radicals or carbon atoms. Since the C 1s peak at 286.0 eV for CO/Rh(111) at low coverage is well defined in the literature, the measured data relative to it have been plotted at top panel in Fig. 3, where the calculated SCLSs from the present work are included, too. The agreement between theoretical and experimental data suggests the formation of individual  $\text{CH}_x$  ( $x=1-3$ ) products during the decomposition of the ethanol, which is critical to understand the mechanism of the ethanol dissociation on Rh(111) surfaces.

The calculated work functions for  $\text{CH}_x$  ( $x=1-3$ ) adsorption on the energetically favorable hollow sites with and without the presence of CO are tabulated in Table V and plotted in Fig. 4. The calculated work function  $\Phi$  for the clean Rh(111) surface is 5.27 eV, which agrees well with

TABLE V. C 1s surface core-level shift and variations of work function ( $\Delta\phi$ ) (in eV) for CO molecule and  $\text{CH}_x$  radical on Rh(111) surface within  $(2 \times 2)$  cell. All shifts are relative to the C 1s in the atop CO on Rh(111) calculated in  $(2 \times 2)$  cell.

$\Delta\text{SCLS}/(\text{eV})$				$\Delta\phi/(\text{eV})$			
CO top	CH hcp	$\text{CH}_2$ fcc/bri-H	$\text{CH}_3$ fcc/top-H	CO top	CH hcp	$\text{CH}_2$ fcc/bri-H	$\text{CH}_3$ fcc/top-H
Clean Rh(111)							
0.00	-2.45	-2.21	-1.67	0.72	-0.60	-0.95	-1.31
CO precovered Rh(111)							
...	-2.55	-2.31	-1.85		0.32	0.12	-0.12

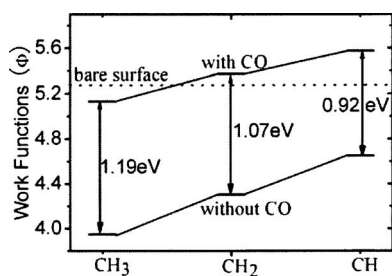


FIG. 4. Variations of work function ( $\Delta\phi$ ) for the  $\text{CH}_x$  ( $x=1-3$ ) adsorbed on clean and CO precovered Rh(111) surfaces at their energetically most favorable sites. The dashed line corresponds to the work function of the clean Rh(111) surface.

experimental measurement, 5.3 eV.<sup>66</sup> As seen from Table V, CO adsorption induces an increase of the work function for the clean surfaces, which indicates a net electron transfer from the substrate to the CO molecule. However, the adsorption of the  $\text{CH}_x$  ( $x=1-3$ ) species induces generally a reduction of the work function ( $\Delta\Phi < 0$ ), which indicates a reverse electron transfer. From  $\text{CH}_3$  to  $\text{CH}$ ,  $\Delta\Phi$  decreases, and electron transfer reduces sequentially. For coadsorption system, the variations of the work functions are a superposition from these two adsorbates, which are shown clearly in Fig. 4. Overall variations of the work function are the reduction by 0.12 eV for  $\text{CH}_3+\text{CO}$ , but increase by 0.12 eV for  $\text{CH}_2+\text{CO}$  and 0.32 eV for  $\text{CH}+\text{CO}$ , respectively.

## VI. VIBRATIONAL FREQUENCIES

For adsorbed  $\text{CH}_2$  and  $\text{CH}_3$  radicals, which can be generated by the thermal and photoinduced dissociations of corresponding iodo compounds, their vibration frequencies are available in literatures and tabulated in Table VI with present calculations. To the best of our knowledge, there is no vibrational data available for  $\text{CH}$  on Rh(111).

For  $\text{CH}_3$  adsorption, the asymmetric stretching mode  $\nu_{\text{as}}(\text{CH}_3)$  is calculated for two different configurations: fcc/top-H and top/top-H. Comparing to  $\nu_{\text{as}}(\text{CH}_3)$  being  $3149\text{ cm}^{-1}$  at top/top-H site, a significant softening is found at fcc/top-H site being  $2871\text{ cm}^{-1}$ . Adsorption induced soft-

ness has been found in various systems, and possible mechanisms involved can be explained either by formation of a multicenter hydrogen-bond-like interaction between C–H and the metal atom underneath (C–H–M bonding) or by partial charge back donation from the substrate to the adsorbed alkane.<sup>15,25</sup> For atop site adsorption, the distance between H and Rh atoms ( $2.65\text{ \AA}$ ) is too large to form any possible bonding, correspondingly; only partial charge back donation from the metal to the molecules may take place, if there is any mode-softening exist. For fcc/top-H configuration, the distance between H atom and metal atoms decreases significantly to  $2.13\text{ \AA}$  and falls well into the range of the typical bond length of the hydrogen bonding. In this case, both mechanisms mentioned above may work. To figure out which mechanism is correct, the difference of charge density has been plotted in Fig. 5. From Fig. 5, considerable charge accumulation between C and metal atoms can be seen immediately, which favors the mechanism of charge back donation from the substrate to the adsorbed radicals. As seen from Table VI, only vibration at fcc/top-H site presents considerable mode softening, which agrees with experimental findings.<sup>10</sup> Since the fcc/top-H site preference is predicted only by PW91, the agreement of the vibration at fcc-hollow sites with respect to the experiment indicates that PW91 functional is proper functional to describe the  $\text{CH}_3$  adsorption on Rh(111), as discussed in above.

For  $\text{CH}_2$  adsorption, the calculated  $\nu_{\text{as}}(\text{CH}_2)$  is  $2987\text{ cm}^{-1}$ , which agrees well with experimental measurement,  $2940\text{ cm}^{-1}$  for  $\text{CH}_2$  adsorption generated from  $\text{CH}_2\text{I}_2$ .<sup>12,13</sup> For  $\text{CH}$  adsorption on Rh(111), the calculated stretching frequency for C–H bond is  $2931\text{ cm}^{-1}$  at the hcp site and  $2951\text{ cm}^{-1}$  at the fcc site. Corresponded experimental measurement is remained. We note that for  $\text{CH}_2/\text{Rh}(111)$ , additional vibrational peak at  $3020\text{ cm}^{-1}$  occurred when temperature was raised to  $450-500\text{ K}$  and was attributed to form  $\text{CH}$ , experimentally.<sup>12</sup>

If CO was preadsorbed on the surfaces, the mode softening for methyl radical is inhibited and results in blueshift by  $43\text{ cm}^{-1}$ . For  $\text{CH}_2$  and  $\text{CH}$ , though the blueshifts are found, the effect is negligible, for example,  $8\text{ cm}^{-1}$  for

TABLE VI. Calculated and available experimental vibrational frequencies (in  $\text{cm}^{-1}$ ) of  $\text{CH}_x$  species on Rh(111) within  $(2\times 2)$  cell. For  $\text{CH}_2$  and  $\text{CH}_3$ , calculated  $\nu(\text{CH}_x)$  is for asymmetric stretching mode; and for  $\text{CH}$ ,  $\nu(\text{CH}_x)$  for C–H stretching mode.

	CH		CH <sub>2</sub>			CH <sub>3</sub>		
	Expt.	Calc.	Expt.	Calc.	Expt.	Calc.		
		hcp				fcc	fcc/top-H	top/top-H
Rh(111)								
$\nu(\text{CH}_x)$	3020 <sup>a</sup>	2931	2951	2940	2987	2920 <sup>a</sup>	2871	3149
$\nu(\text{C-O})$	2040 <sup>b</sup>							
CO precovered Rh(111)								
$\nu(\text{CH}_x)$	...	2931	2954	2960	2995	~2958 <sup>c</sup>	2914	
$\nu(\text{C-O})$	...	2055	2051	...	2032	2020 <sup>c</sup>	2016	

<sup>a</sup>Reference 10.

<sup>b</sup>Reference 56.

<sup>c</sup>Reference 12.

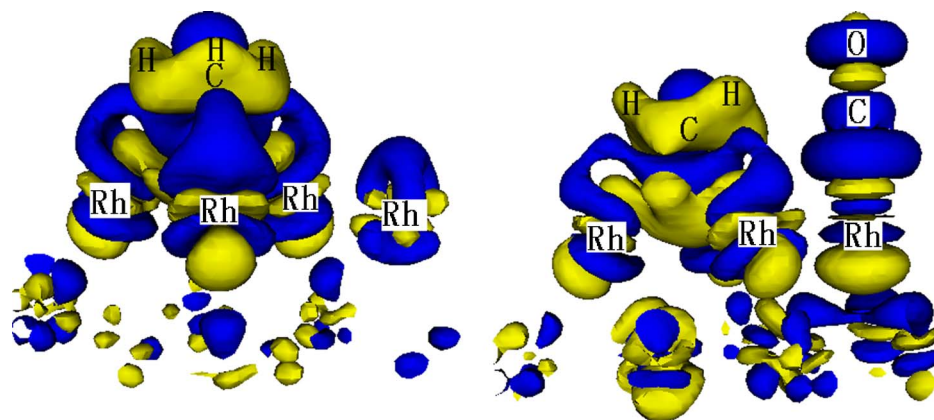


FIG. 5. (Color online) Isosurface of difference of electron densities for adsorbed  $\text{CH}_3$  (fcc-hollow site) on clean and CO precovered Rh(111) surfaces. The yellow and blue colors indicate electron depletion and accumulation, respectively.

$\nu_{\text{as}}(\text{CH}_2)$  and  $3 \text{ cm}^{-1}$  for  $\nu(\text{CH})$ , respectively. The CO induced blueshift of methyl group comes from the weakened interaction between methyl and substrate due to the repulsion between adsorbates. As known from Blyholder theory,<sup>67</sup> the chemisorptions of CO on transition metal surfaces occur through electron transfer from the CO 5 $\sigma$  orbital to the metal and back donation of substrate electrons to the empty  $2\pi^*$  orbital of CO. The electron depletion from the metal surface due to back donation toward CO, as indicated by the increase of the work function discussed above, weakens the carbon and metal bond. To make this point clear, the difference of the charge density with the presence of CO has been plotted and given on the right of Fig. 5. Compared to the pure methyl adsorption (left panel), the charge accumulation between C in  $\text{CH}_3$  and Rh atoms decreases considerably. Experimentally,  $\nu_{\text{as}}(\text{CH}_3)$  with and without the presence of CO has been measured by Kecskés *et al.*,<sup>10</sup> and the blueshift with magnitude of  $40 \text{ cm}^{-1}$  induced by the presence of CO was found, which agrees well with the present calculations. For adsorbed  $\text{CH}_3$  on Rh(111), the blueshift has been found when oxygen was preplaced on the surfaces by both of experimental measurement<sup>6</sup> and theoretical calculation.<sup>25</sup> The mechanism behind is exactly same: the repulsive interactions between methyl and coadsorbates (O in their cases and CO in present case) are built up, and the coupling between methyl and the substrate is weakened, and mode softness is relived.

Conversely, C–O stretch is affected by coadsorbed  $\text{CH}_x$  radicals too. For atop CO adsorption at  $1/4 \text{ ML}$ , calculated  $\nu(\text{CO})$  is  $2073 \text{ cm}^{-1}$  from the present work. Using six-layer slab, Köhler *et al.* obtained  $2015 \text{ cm}^{-1}$  (GGA) and  $2027 \text{ cm}^{-1}$  (GGA+U),<sup>53</sup> while experimental measurement is  $2040 \text{ cm}^{-1}$ .<sup>56</sup> The agreement is good. With the presence of methyl, both of experimental measurements<sup>10</sup> and present calculations find considerable softness for C–O stretch ( $56 \text{ cm}^{-1}$  for previous one and  $57 \text{ cm}^{-1}$  for the later one), which is stark contrast to the inhibition of the redshift of methyl vibration with the presence of CO, as found above. The reason can be attributed to the effect of inversed charge transfer. As seen from the variation of the work function methyl groups, acting as an electron donor, induce the reduction of the work function, while adsorbed CO increases work function as an electron acceptor. When both molecules adsorb on the surface, donated electron from  $\text{CH}_3$  facilitates/enhances the electron back donation from the substrate to the

$2\pi^*$  antibonding state of adsorbed CO. The C–O bond is thus weakened and C–O stretching is softened, correspondingly. Recently, Krenn *et al.*<sup>26</sup> studied in detail on CO and O coadsorptions on Rh(111) by RAIRS and DFT. After introducing oxygen, blueshift for C–O stretching has been found. This is because both oxygen and CO attempt to take electrons from the substrate, as evidenced from increasing of the work function for adsorption of these two individual molecules. The charge competition between these two coadsorbates results in less charge transfer from the substrate into the antibonding state of CO, and thus the C–O bond is strengthened and the C–O stretch softness is prevented. These analyses indicate that it is likely to tune the adsorbed molecule activity through the mediation of the substrate simply by placing molecules with opposite electronic properties (for example, electron negativity) nearby.

## VII. PROJECTED DENSITY OF STATES

To gain deep insight into the interactions between the adsorbates and surfaces, projected density of states (PDOS) is plotted and shown in Fig. 6. For simplicity, only PDOS for all  $\text{CH}_x$  adsorbed at fcc-hollow sites is considered. The C  $2p$  orbitals, H  $1s$  orbitals, and  $4d$  bands of surface Rh atoms bonded to adsorbed molecules are shown. From Fig. 6, hybridization between C  $2p$  orbital and Rh  $4d$  band can be found, in general.

For CH adsorption on the clean Rh(111), one marked peak at the lower side of Rh  $4d$  band and C  $2p$  orbital indicates a pronounced hybridization between them. By examining individual components of the orbitals, it has been found that the hybridization comes mainly from C  $2p_z$  and Rh  $d_{x^2-y^2}$  and  $d_{z^2}$  orbitals. The population of C  $2p_x$  and  $2p_y$  orbitals is modest. Co adsorption of CO does not cause any considerable change toward the bonding between CH and substrates.

For  $\text{CH}_2$  adsorption, the in-plane symmetry is broken. Compared to adsorbed CH, C  $2p_y$  is now participated into the hybridization with Rh  $4d$  band, and the C  $2p_z$  is broadened. With increase of the hydrogen atom number from CH to  $\text{CH}_3$ , the contribution from H  $1s$  orbital increases correspondingly. By checking the PDOS carefully, it has been found that the interaction comes from the hybridization between C  $2p_z$ ,  $2p_y$  orbitals, and Rh  $d_{x^2-y^2}$ ,  $d_{z^2}$ , and  $d_{yz}$  bands.

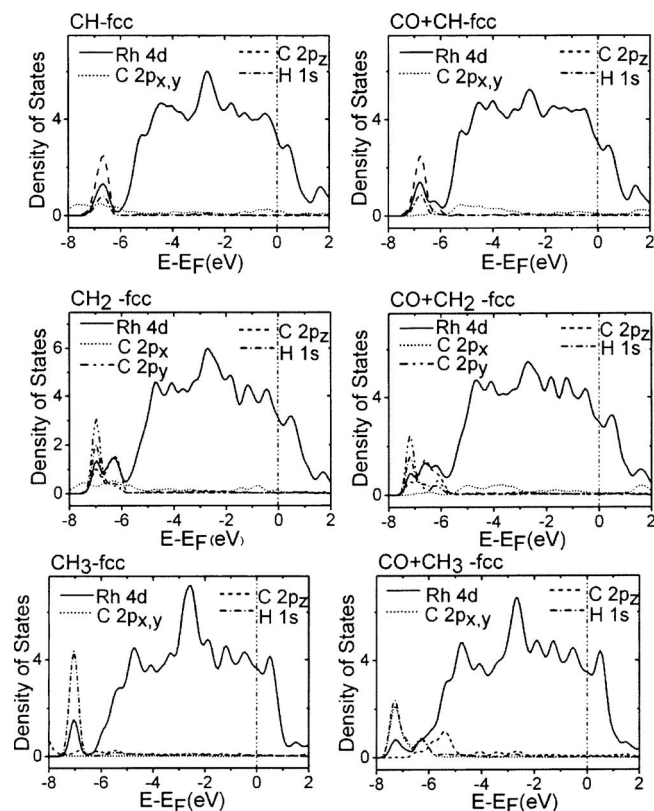


FIG. 6. Density of states projected on the H  $1s$ , C  $2p$ , and Rh  $4d$  orbitals for adsorbed  $\text{CH}_x$  on clean and CO precovered Rh(111) surfaces. The energy reference is Fermi energy, indicated by the vertical dashed-dotted line.

For  $\text{CH}_3$  adsorption, due to the higher  $C_{3v}$  symmetry which is lacking in the  $\text{CH}_2$  adsorption, the  $C 2p_x$  and  $C 2p_y$  orbitals become equivalent, and both of them participate in the interaction with surface Rh atoms.

### VIII. CONCLUSION

$\text{CH}_x$  ( $x=1-3$ ) adsorptions on clean and CO precovered Rh(111) surfaces were systematically studied by density functional theory calculations. It is found that  $\text{CH}_x$  ( $x=1-3$ ) radicals prefer threefold hollow site, in general, on clean and CO precovered Rh(111) surfaces. The interaction strength between  $\text{CH}_x$  and the metal surfaces follows the order of  $\text{CH}_3 < \text{CH}_2 < \text{CH}$ . There is attractive interaction between adsorbed  $\text{CH}_x$  at low coverage between  $1/9$  and  $1/4$  ML, and significant repulsions are built up when the coverage increase further.

The electronic structure analysis shows that there is considerable charge transfer from the adsorbed  $\text{CH}_x$  ( $x=1-3$ ) radicals to the substrate, accompanied by the reduction of the work function. For  $\text{CH}_3$  adsorption, charge accumulation between carbon atom and the surface Rh atom underneath is identified.

The charge back donation from the substrate to the adsorbed  $\text{CH}_x$  ( $x=1-3$ ) accounts for the mode softening of the C-H stretching vibrations, which may have important implication on their reactivities. However, the interaction between  $\text{CH}_x$  ( $x=1-3$ ) and the substrate is weakened due to the repulsive interaction between adsorbates, which prevents the mode softening of the C-H stretching vibration in  $\text{CH}_3$ . On

the other hand, overall charge transfer from  $\text{CH}_3$  and  $\text{CH}_2$  to the substrate facilitates/enhances the back donation from the substrate to CO, which results in the mode softening for the C-O stretch.

### ACKNOWLEDGMENTS

One of the authors (W.X.L.) gratefully acknowledge the financial support from the National Natural Science Foundation of China (No. 20503030) and Chinese Academy of Sciences "Bairen Project." Another authors (X.H.B.) thanks the financial support from the National Natural Science Foundation of China (No. 90206036) and the Ministry of Science and Technology of China (2005CB221405). The authors thank Jason White from UCSB for going through the manuscript.

- <sup>1</sup> H. Trevino, G. D. Lei, and W. M. H. Sachtler, *J. Catal.* **154**, 245 (1995).
- <sup>2</sup> S. S. C. Chuang, R. W. Stevens, and R. Khatri, *Top. Catal.* **32**, 225 (2005).
- <sup>3</sup> Y. Wang, H. Y. Luo, D. B. Liang, and X. H. Bao, *J. Catal.* **196**, 46 (2000).
- <sup>4</sup> M. Mavrikakis, M. Bäumer, H.-J. Freund, and J. K. Nørskov, *Catal. Lett.* **81**, 153 (2002).
- <sup>5</sup> F. Buatier de Mongeot, A. Toma, A. Molle, S. Lizzit, L. Petaccia, and A. Baraldi, *Phys. Rev. Lett.* **97**, 056103 (2006).
- <sup>6</sup> C. W. J. Bol and C. M. Friend, *J. Am. Chem. Soc.* **117**, 8053 (1995).
- <sup>7</sup> F. Solymosi and G. Klivényi, *J. Electron Spectrosc. Relat. Phenom.* **64**, 499 (1993).
- <sup>8</sup> J. Kiss, A. Kis, and F. Solymosi, *Surf. Sci.* **454/456**, 273 (2000).
- <sup>9</sup> L. Bugyi, A. Oszkó, and F. Solymosi, *J. Catal.* **159**, 305 (1996).
- <sup>10</sup> T. Kecskés, R. Barthos, J. Raskó, and J. Kiss, *Vacuum* **71**, 107 (2003).
- <sup>11</sup> F. Solymosi, *J. Mol. Catal. A: Chem.* **131**, 121 (1998).
- <sup>12</sup> G. Klivényi and F. Solymosi, *Surf. Sci.* **342**, 168 (1995).
- <sup>13</sup> F. Solymosi and G. Klivényi, *J. Phys. Chem.* **99**, 8950 (1995).
- <sup>14</sup> E. Vesselli, A. Baraldi, G. Comelli, S. Lizzit, and R. Rosei, *ChemPhysChem* **5**, 1133 (2004).
- <sup>15</sup> A. Michaelides and P. Hu, *J. Chem. Phys.* **114**, 2523 (2001).
- <sup>16</sup> A. Michaelides and P. Hu, *Surf. Sci.* **437**, 362 (1999).
- <sup>17</sup> H. Yang and J. L. Whitten, *J. Am. Chem. Soc.* **113**, 6442 (1991).
- <sup>18</sup> M. Chen, C. M. Friend, and R. A. van Santen, *Catal. Today* **50**, 621 (1999).
- <sup>19</sup> J. E. Demuth, H. Ibach, and S. Lehwald, *Phys. Rev. Lett.* **40**, 1044 (1978).
- <sup>20</sup> M. A. Chesters, S. F. Parker, and R. Raval, *J. Electron Spectrosc. Relat. Phenom.* **39**, 155 (1986).
- <sup>21</sup> R. Raval and M. A. Chesters, *Surf. Sci.* **219**, L505 (1989).
- <sup>22</sup> E. Cooper, A. M. Coats, and R. Raval, *J. Chem. Soc., Faraday Trans.* **91**, 3703 (1995).
- <sup>23</sup> W. X. Huang, Z. Q. Jiang, and J. M. White, *Chem. Phys. Lett.* **428**, 293 (2006).
- <sup>24</sup> H. Y. Xiao and D. Q. Xie, *Surf. Sci.* **558**, 15 (2004).
- <sup>25</sup> E. J. Walter and A. M. Rappe, *Surf. Sci.* **549**, 265 (2004).
- <sup>26</sup> G. Krenn, I. Bako, and R. Schennach, *J. Chem. Phys.* **124**, 144703 (2006).
- <sup>27</sup> M. Mavrikakis, J. Rempel, J. Greeley, L. B. Hansen, and J. K. Nørskov, *J. Chem. Phys.* **117**, 6737 (2002).
- <sup>28</sup> D. C. Ford, Y. Xu, and M. Mavrikakis, *Surf. Sci.* **587**, 159 (2005).
- <sup>29</sup> I. M. Ciobica, F. Frechard, R. A. van Santen, A. W. Kley, and J. Hafner, *Chem. Phys. Lett.* **311**, 185 (1999).
- <sup>30</sup> I. M. Ciobica, F. Frechard, R. A. van Santen, A. W. Kley, and J. Hafner, *J. Phys. Chem. B* **104**, 3364 (2000).
- <sup>31</sup> C.-T. Au, M.-S. Liao, and C.-F. Ng, *Chem. Phys. Lett.* **267**, 44 (1997).
- <sup>32</sup> C.-T. Au, C.-F. Ng, and M.-S. Liao, *J. Catal.* **185**, 12 (1999).
- <sup>33</sup> A. D. Koster and R. A. Van Santen, *J. Catal.* **127**, 141 (1991).
- <sup>34</sup> J.-F. Paul and P. Sautet, *J. Phys. Chem. B* **102**, 1578 (1998).
- <sup>35</sup> J. Kua and W. A. Goddard III, *J. Phys. Chem. B* **102**, 9492 (1998).
- <sup>36</sup> T. Jacob and W. A. Goddard III, *J. Phys. Chem. B* **109**, 297 (2005).
- <sup>37</sup> A. Michaelides and P. Hu, *J. Chem. Phys.* **112**, 8120 (2000).
- <sup>38</sup> J. Robinson and D. P. Woodruff, *Surf. Sci.* **498**, 203 (2002).
- <sup>39</sup> M. Pascal, C. L. A. Lamont, M. Kittel, J. T. Hoeft, L. Constant, M.

- Polcik, A. M. Bradshaw, R. L. Toomes, and D. P. Woodruff, *Surf. Sci.* **512**, 173 (2002).
- <sup>40</sup>R. M. Watwe, H. S. Bengaard, J. R. Rostrup-Nielsen, J. A. Dumesic, and J. K. Nørskov, *J. Catal.* **189**, 16 (2000).
- <sup>41</sup>G. C. Wang, J. Li, X. F. Xu, R. F. Li, and J. Nakamura, *J. Comput. Chem.* **26**, 871 (2005).
- <sup>42</sup>B. Hammer, L. B. Hansen, and J. K. Nørskov, *Phys. Rev. B* **59**, 7413 (1999).
- <sup>43</sup>J. A. White and D. M. Bird, *Phys. Rev. B* **50**, 4954 (1994).
- <sup>44</sup>J. P. Perdew, J. A. Chevary, S. H. Vosko, K. A. Jackson, M. R. Pederson, D. J. Singh, and C. Fiolhais, *Phys. Rev. B* **46**, 6671 (1992).
- <sup>45</sup>J. Neugebauer and M. Scheffler, *Phys. Rev. B* **46**, 16067 (1992).
- <sup>46</sup>D. C. Harris and M. D. Bertolucci, *Symmetry and Spectroscopy: An Introduction to Vibrational and Electronic Spectroscopy* (Oxford University Press, Oxford, 1978).
- <sup>47</sup>D. Curulla, R. Linke, A. Clotel, J. M. Ricart, and J. W. Niemantsverdriet, *Chem. Phys. Lett.* **354**, 503 (2002).
- <sup>48</sup>S. González, C. Sousa, and F. Illas, *Surf. Sci.* **531**, 39 (2003).
- <sup>49</sup>S. González, C. Sousa, and F. Illas, *J. Phys. Chem. B* **109**, 4654 (2005).
- <sup>50</sup>K. P. Huber and G. Herzberg, *Molecular Spectra and Molecular Structure, Constants of Diatomic Molecules* (Van Nostrand-Reinhold, New York, 1979), Vol. 4.
- <sup>51</sup>J. G. Wang, W. X. Li, M. Borg *et al.*, *Phys. Rev. Lett.* **95**, 256102 (2005).
- <sup>52</sup>M. Birgersson, C.-O. Almbladh, M. Borg, and J. N. Andersen, *Phys. Rev. B* **67**, 045402 (2003).
- <sup>53</sup>L. Köhler and G. Kresse, *Phys. Rev. B* **70**, 165405 (2004).
- <sup>54</sup>M. Smedh, A. Beutler, T. Ramsvik, R. Nyholm, M. Borg, J. N. Andersen, R. Duschek, M. Sock, F. P. Netzer, and M. G. Ramsey, *Surf. Sci.* **491**, 99 (2001).
- <sup>55</sup>P. J. Feibelman, B. Hammer, J. K. Nørskov, F. Wagner, M. Scheffler, R. Stumpf, R. Watwe, and J. Dumesic, *J. Phys. Chem. B* **105**, 4018 (2001).
- <sup>56</sup>R. Linke, D. Curulla, M. J. P. Hopstaken, and J. W. Niemantsverdriet, *J. Chem. Phys.* **115**, 8209 (2001).
- <sup>57</sup>I. Grinberg, Y. Yourdshahyan, and A. Rappe, *J. Chem. Phys.* **117**, 2264 (2002).
- <sup>58</sup>M. Gajdos, A. Eichler, and J. Hafner, *J. Phys.: Condens. Matter* **16**, 1141 (2004).
- <sup>59</sup>E. Shustorovich, *Surf. Sci. Rep.* **6**, 1 (1998).
- <sup>60</sup>N. Brønsted, *Chem. Rev. (Washington, D.C.)* **5**, 231 (1928).
- <sup>61</sup>M. G. Evans and N. P. Polanyi, *Trans. Faraday Soc.* **34**, 11 (1938).
- <sup>62</sup>A. Kokalj, N. Bonini, C. Sbraccia, S. de Gironcoli, and S. Baroni, *J. Am. Chem. Soc.* **126**, 16732 (2004).
- <sup>63</sup>R. C. Egeberg, S. Ullmann, I. Alstrup, C. B. Mullins, and I. Chorkendoff, *Surf. Sci.* **497**, 183 (2002).
- <sup>64</sup>B. S. Bunnik and G. J. Kramer, *J. Catal.* **242**, 309 (2006).
- <sup>65</sup>A. Beutler, E. Lundgren, R. Nyholm, J. N. Andersen, B. J. Setlik, and D. Heskett, *Surf. Sci.* **396**, 117 (1998).
- <sup>66</sup>P. Brault, H. Range, J. P. Toennies, and Ch. Wöll, *Z. Phys. Chem. (Munich)* **198**, 1 (1997).
- <sup>67</sup>G. Blyholder, *J. Phys. Chem.* **68**, 2772 (1964).